Journal of Magnetic Resonance 307 (2019) 106565

Contents lists available at ScienceDirect

Journal of Magnetic Resonance

journal homepage: www.elsevier.com/locate/jmr

Optimized inside-out magnetic resonance probe for soil moisture measuring in situ

Sheng Shen [a], Pan Guo [b], Jiamin Wu [a], Ye Ding [a], Fangge Chen [a], Fanqin Meng [a], Zheng Xu [a,*]

[a] State Key Laboratory of Power Transmission Equipment and System Security and New Technology, Chongqing University, Chongqing 400044, China
[b] School of Physics and Electronic Engineering, Chongqing Normal University, Chongqing 401331, China

ARTICLE INFO

Article history:
Received 14 May 2019
Revised 23 July 2019
Accepted 24 July 2019
Available online 25 July 2019

Keywords:
Inside-out NMR probe
Permanent magnet optimization
RF coil optimization
Soil moisture

ABSTRACT

We report a novel inside-out NMR (nuclear magnetic resonance) probe for the measurement of soil moisture. The probe consists of a dumbbell-shape magnet and an opposed-solenoid RF (radio frequency) coil. Optimization methods for the structure of the magnet and RF coil that maximize the SNR (signal-to-noise ratio) of NMR measurements are also described. The dumbbell-shape magnet consists of three cylindrical magnets in series whose magnetic field was calculated with analytic expression deduced by converting magnet to equivalent magnetization current on its cylindrical surface. Based on the analytic expression, a nonlinear optimization mathematical model was built to determine the optimal structure parameters automatically. The opposed-solenoid is a pair of reverse-connected solenoids and used as RF coil on inside-out NMR probe in this work. Its structure-parameter optimization was carried out based on FEM (finite element method) simulation, and UD (uniform design) was applied to increase the optimization efficiency. A prototype was designed and built consisting of a magnet with length of 100 mm and a diameter of 40 mm. An NMR-based soil moisture measuring experiment was conducted by this prototype, with NMR performed using the CPMG (Carr-Purcell-Meiboom-Gill) pulse sequence for soil sample in different moisture content. The T_2 distribution spectrum reveals that there are two compartments of water in the soil sample: free water and bound water.

1. Introduction

Soil moisture (i.e water) is an inevitable part of the three phases system of the soil, which comprises of soil minerals (solids), moisture and air [1,2]. It has a major role to play as far as the plant growth [3]. In agriculture practice, the application of adequate and timely moisture for irrigation is essential in crop production, and its schedule depends upon the soil-moisture-plant environment [4–7]. So, accurate accessing of the soil-moisture-plant environment plays an essential role in agriculture. Indeed, a firm quantitative description of the phenomena of moisture in soils and the factors which are part of it will greatly advancement of deeper understanding in soil hydrology.

The requirement for accurate soil-moisture measurement has led to the emergence of experimental techniques such as Time Domain Reflectometry (TDR) [8], Neutron Absorption [9] or Electrical Impedance Tomography [10]. Over the past decades, these techniques demonstrated their utility. Nevertheless, they are not free of drawbacks: their results for soil moisture can also be adversely affected by local ion concentration in water and the changes induced by the actual presence of the sensor. NMR (Nuclear Magnetic Resonance) measurement is non-invasive; it would not affected by ion concentrations, which is determined by the physical principle it relies on. Besides the mere moisture content, the local dynamics of the liquid in the pore system can also be observed by it [11].

The advent of NMR performed with highly inhomogeneous low magnetic fields traces back to the pioneering work of Jasper Jackson in 1980 [12–20] where the concept of "inside-out" was first proposed. This work advanced the early work of Brown and Gamson in creating a NMR well-logging tool (NWL) based on earth field in 1960s, overcoming the long "deadtime" of NWL and the fact that measurements were subject to being perturbed by the presence of drilling mud in the borehole [21,22]. The measurement of soil moisture via NMR, though it was among the first applications of low-field instruments [23], has not been developed to the same level as in well-logging applications.

Low-field NMR certainly can play an important role in the future of soil moisture measurement. A promising example of this is given by the NMR-sounding technique, which has successfully been applied in the search of aquifers in the last 10 years [24].

* Corresponding author.
E-mail address: xuzheng@cqu.edu.cn (Z. Xu).

https://doi.org/10.1016/j.jmr.2019.07.052
1090-7807/

Recently, several NMR probes for water moisture measurement were proposed. Perlo [25] and Wu [26] analyzed different structures of low-field NMR probe, and discussed their performance. However the published work did not develop any method to optimize the structure of NMR probe. In this paper, we propose a novel geometry inside-out NMR probe, including the development of different methods to optimize the structure of the magnet and RF coil.

The probe consists of a dumbbell-shape magnet and opposed-solenoid RF coil. The dumbbell-shape magnet can be applied on inside-out probe with magnetization along radial direction or longitudinal direction, its static magnetic field in ROI (region of interest) could be optimized by adjusting the structure parameter of magnet [25–27]. In the presently described work, the dumbbell-shape magnet was exploited with magnetization along longitudinal direction. To optimize the structure, we deduced an analytic expression of magnetic field generated by dumbbell-shape magnet, that makes it possible to describe the optimization problem using an analytic mathematical model, which could be solved automatically in commercial mathematical computing software with high efficiency and precision. Based on the analytic magnetic field expression, we converted the structure parameter optimization to a nonlinear optimization problem which was solved using function *fmincon* in MATLAB (The MathWorks, Inc.).

The structure of probe we studied in this paper is a solid of revolution. RF coils, designed for revolved-body probe, are usually solenoid and saddle coil. The structure of first inside-out NMR probe is also a solid of revolution; the RF coil is a solenoid [12,13]. Additionally, different saddle RF coils were developed to match revolved-body magnet which is magnetized in different directions [20,25,26,28]. In this paper, we propose a novel RF coil: opposed-solenoid with a differential structure that can reduce coupling noise in space and benefit the SNR of NMR measurement [29,30]. Moreover, both the ROI of the probe and the opposed-solenoid RF coil are solids of revolution, and compared to the saddle RF coil, the RF magnetic field of an opposed-solenoid RF coil can be more homogeneous, and match the static magnetic field ROI better. We also optimized the structure of RF coil and that was carried out based on the analysis of its magnetic field distribution and AC (alternative current) resistance. However, because of the influence of eddy current in magnet shielding, it is hard to calculate magnetic field and AC resistance precisely with analytical method. In this paper, we calculate these parameters with FEM (finite element method) simulation which could provide precise result but also require large hardware and time cost. In order to improve the optimization efficiency, UD (uniform design), an experiment design method, was used to design simulation and analyze simulation results.

To verify the design and optimization methods, we also made a prototype with magnet height of 100 mm, diameter of 40 mm, and conducted soil moisture measuring experiments. We set up soil samples with different moisture content; NMR measurements were evaluated by analyzing the relation between NMR signal and soil moisture content of sample.

2. Method

The magnet to be optimized is shown as Fig. 1(a), with a magnetic axis along its axial direction. Gray ring in Fig. 1(b) indicates the ROI. The direction of $\boldsymbol{B_0}$ (static magnetic field) around the magnet is parallel to the axis. Because the SNR of NMR measurement is proportional to B_0^2 [31], the goal of magnet optimization is to maximize the static magnetic field strength with required homogeneity in ROI. The structure parameters, to be optimized, were shown as Fig. 1(c), where D_1, H_1 are the diameter and height of the magnet in the end, and D_2, H_2 are the diameter and height of magnet in the middle. In this paper, the parameter optimization was converted to a nonlinear optimization problem, introduced in 2.1.

The RF coil needs to generate an AC magnetic field ($\boldsymbol{B_1}$) which is orthogonal to static magnetic field ($\boldsymbol{B_0}$) generated by the magnet. The opposed-solenoid RF coil, shown as Fig. 2(a), consists of two reverse-connected solenoids, and it was applied on inside-out NMR probe for the first time in this paper. Basically, $\boldsymbol{B_1}$, the RF magnetic field, is along the radial direction of dumbbell-shape magnet, and that is orthogonal to the static magnetic field $\boldsymbol{B_0}$. Considering that only a reasonable design with an optimal structure could make the RF coil to maximize the SNR in NMR measurement, the coil structure parameters should be optimized, and that include the number of turns *X1*, turn spacing *X2*, and the gap between two solenoids *X3*, shown as Fig. 2(b). Fig. 3 shows the electromagnetic structure of the probe, $\boldsymbol{I}$ denotes current in RF coil; the vector distributions of $\boldsymbol{B_0}$ and $\boldsymbol{B_1}$ are in a rotating plane of ROI. Because both the magnet and ROI are solids of revolution, magnetic field distribution in space could be reflected by analyzing that in the rotating plane.

2.1. Magnet optimization

Magnet optimization was carried out based on calculation of its magnetic field distribution. In this paper, we introduced equivalent magnetization current method to calculate it with analytic expression. As is shown in Fig. 4, we replaced the source of $\boldsymbol{B_0}$ from cylindrical magnet, with magnetization along its axis, to current density $\boldsymbol{K}$ on cylindrical surface of the magnet. Then, $\boldsymbol{B_0}$ could be regarded as that generated by surface current density $\boldsymbol{K}$, and it could be calculated according to Biot-Savart law, shown as Eqs. (2)–(6). K could be obtained by Eq. (1), where B_r is the residual flux density of permanent magnet, B_r is permeability of free space μ_0 is permeability of free space ($4\pi \times 10^{-7}$ H/m) [32].

$$K = B_r/\mu_0 \tag{1}$$

Then, $\boldsymbol{B_0}$ at any point P (x_0,y_0,z_0) in the space was calculated according to Biot-Savart law, and the components of 3 directions were expressed as Eqs. (2)–(4):

$$B_x = \frac{B_r dz}{4\pi}\int_Z^{Z+H}\int_0^{2\pi}\frac{R(z_0 - z)\cos\theta}{K_m}d\theta \tag{2}$$

$$B_y = \frac{B_r dz}{4\pi}\int_Z^{Z+H}\int_0^{2\pi}\frac{R(z_0 - z)\sin\theta}{K_m}d\theta \tag{3}$$

$$B_z = -\frac{B_r dz}{4\pi}\int_Z^{Z+H}\int_0^{2\pi}\frac{R[(x_0 - R\cos\theta)\cos\theta + (y_0 - R\sin\theta)\sin\theta]}{K_m}d\theta \tag{4}$$

$$K_m = [(x - R\cos\theta) + (y - R\sin\theta) + (z - z_0)]^{\frac{3}{2}} \tag{5}$$

where (R,θ,z_0) is the corresponding coordinate of (x_0,y_0,z_0) in cylindrical-coordinate system. Flux density module value is calculated by:

$$B_0 = \sqrt{B_x^2 + B_y^2 + B_z^2} \tag{6}$$

The dumbbell-shape magnet consists of 3 cylindrical magnets, and the magnetic field distribution can be calculated by the superposition of magnetic field generated by all cylinder magnets. Based on the analytic expression of magnetic field, we can build a nonlinear optimization model to optimize the structure parameters, D_1, H_1, D_2, H_2, as is shown in Fig. 1(c).

Because the SNR of NMR signal is proportional to B_0^2, and also influenced by magnetic field homogeneity in ROI [31]. Nonlinear

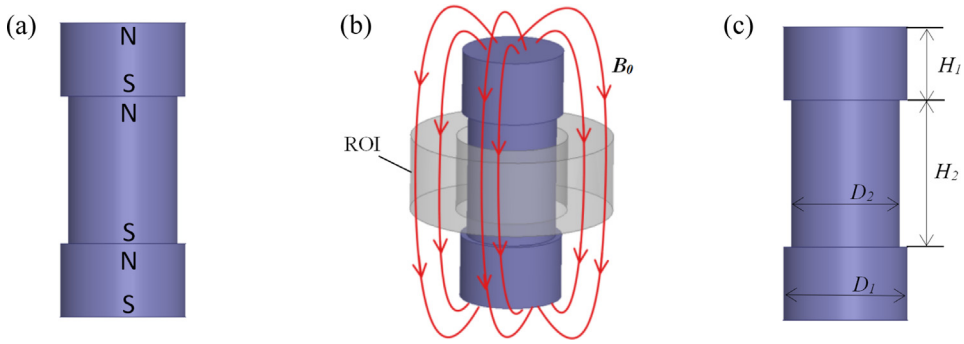

Fig. 1. Dumbbell-shape Magnet. (a) The structure of magnet. (b) The ROI and magnetic field distribution of the magnet. (d) Structure parameter of the magnet.

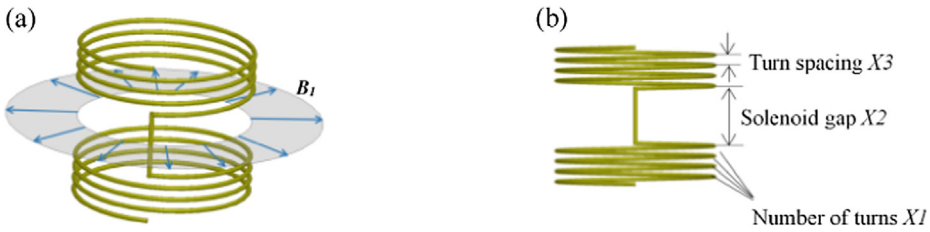

Fig. 2. RF coil. (a) RF coil and RF magnetic field distribution. (b) Structure parameter of RF coil.

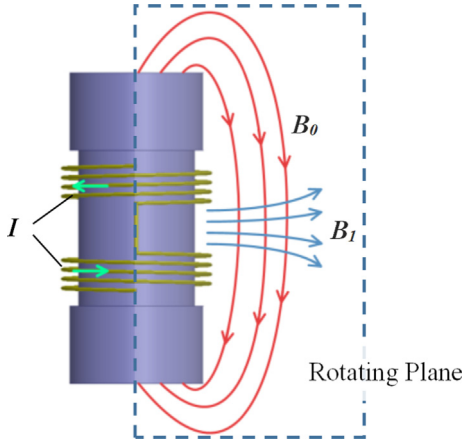

Fig. 3. NMR probe. ***I*** indicates the current in RF coil. Vector distribution of $\boldsymbol{B_0}$ and $\boldsymbol{B_1}$ was shown in the rotating plane.

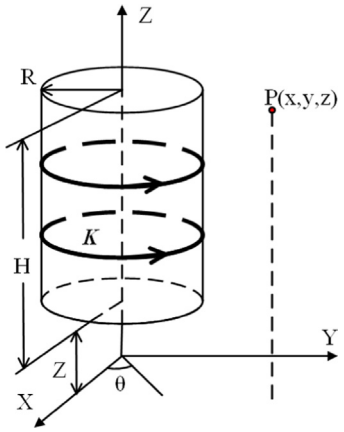

Fig. 4. Equivalent magnetization method. Cylindrical magnet with magnetization along its axis is equivalent to the surface current density K.

optimization was built to find a structure which generates maximum magnetic field strength with certain homogeneity which defined as standard deviation of magnetic flux density in ROI. Nonlinear Optimization problem was described as (7).

$$\text{Maximum}: f(x) = \frac{1}{n}\sum_{i=1}^{n} B_i(D_1, H_1, D_2, H_2)$$

Subject to :

$$\begin{cases} \sqrt{\frac{1}{n}\sum_{i=1}^{n}\left(B_i(D_1,H_1,D_2,H_2) - \frac{1}{n}\sum_{i=1}^{n}B_i(D_1,H_1,D_2,H_2)\right)} \leqslant \sigma \\ H_1 + 2\cdot H_2 \leqslant H_{\max} \\ D_1 \leqslant D_{\max} \\ D_2 \leqslant D_{\max} \end{cases} \tag{7}$$

where B_i is the magnetic flux density at test points, chosen uniformly in ROI; σ is the limitation of standard deviation of magnetic flux density in ROI; H_{max}, D_{max} are the limitations of magnet length and diameter, respectively. Objective function $f(x)$ calculates average value of magnetic flux density at test points, the optimization target is to maximize magnetic field strength in ROI. Homogeneity requirements and magnet size requirements have been reflected in the constraints.

2.2. RF coil optimization based on uniform design (UD)

The RF coil was optimized based on FEM simulation which can be implemented on many choices of commercial software, such as COMSOL Multiphysics (COMSOL Inc.), ANSYS Maxwell (Ansys Inc.), and CST (Dassault Systèmes SIMULIA Corp.). Generally, a large number of simulations and analysis are required for the optimization leading to a high-cost in human and hardware resources. To improve optimization efficiency, UD was introduced to optimize the coil and that could make it optimized with a reasonable number of simulations.

UD is one kind of space filling approach that can be used for designing simulation and experiments. It seeks design points to be uniformly scattered on the experimental domain. Suppose there

are s parameters of interest over a domain C^S. The goal here is to choose a set of m points Pm = {1, . . ., m} ⊂ C^S such that these points are uniformly scattered on C^S [33]. Study on problem in a certain experimental domain could be conducted by analyzing a set of uniformly scattering points in it instead of all the experimental domain. That provides a way to choose typical points in experimental domain, and make conclusion just by analyzing these points.

UD, applied in RF coil optimization, was implemented by following steps [33]:

(1) Choose a parameter (or factor in design terminology) search domain, determine a suitable number of levels for each parameter.
(2) Choose a suitable UD table to accommodate the number of parameters and levels. This can be easily done by visiting the UD-web. http://www.math.hkbu.edu.hk/UniformDesign. UD table is described as $U_n(q^m)$, where U, n, q and m stand for the UD, the number of experimental trials, the number of levels and the maximum number of factors, respectively.
(3) From the UD table, randomly determine the run order of simulations and conduct the simulations.
(4) Quantify performance measure, find the best parameter combination that maximize or minimize the performance measure.
(5) Adjust experiment domain according to existing results, and conduct further follow-up simulation.

We describe here an example of RF coil optimization using UD. The are 3 factors need to be considered in the optimization, shown as Fig. 2(c), the number of turns *X1*, solenoid gap *X2*, and turn spacing *X3*. The experiment domain (*X1,X2,X3*) was chosen as [1,10] × [4,40] × [0.5, 5], where the unit of *X2* and *X3* is mm; the level was set to 10; experimental domain with level of 10 is shown in Table 1. If we analyze all the experimental domain, 3 factors with level of 10 would need 1000 (10^3) simulations, while UD provides a way to analyze and optimize with 10 simulations.

These simulations were arranged with a UD table $U_{10}(10^3)$, as is listed in Table 2. Specifically, the heading of (**1,2,3**) in Table 2 represents uniform design table for 3 factors in 10 runs. The heading of (*X1,X2,X3*) in Table 2 represents the actual experiment values for these three factors. For example, the first combination under heading (**1,2,3**) is (1,5,7), which represent the 1st level of *X1*, 5th level of *X2* and 7th level of *X3*, the corresponding parameters is *X1* = 1, *X2* = 20 and *X3* = 3.5.

All the simulations were conducted according to the UD table, and the best structural parameter was chosen from 10 parameter combinations according to the result of FEM simulation. The performance measure of RF coil was quantified by SNR [31]. Considering that the electromagnetic design focus on magnetic filed distribution and AC resistance of RF coil, for simplicity, we use simplified SNR to evaluate the performance of RF coil which is named as sSNR, shown as Eq. (8).

Table 1
Experiment domain with level of 10.

X1	*X2*	*X3*
1	4	0.5
2	8	1
3	12	1.5
4	16	2
5	20	2.5
6	24	3
7	28	3.5
8	32	4
9	36	4.5
10	40	5

Table 2
$U_{10}(10^3)$ and corresponding design.

No.	1	2	3	*X1*	*X2*	*X3*
1	1	5	7	1	20	3.5
2	2	10	3	2	40	1.5
3	3	4	10	3	16	5
4	4	9	6	4	36	3
5	5	3	2	5	12	1
6	6	8	9	6	32	4.5
7	7	2	5	7	8	2.5
8	8	7	1	8	28	0.5
9	9	1	8	9	4	4
10	10	6	4	10	24	2

$$\mathrm{sSNR} = \int_V \frac{B_0^2 (B_1/I)\cos\theta}{\sqrt{R}} dv \tag{8}$$

where V is the volume of ROI; R is AC resistance of RF coil; and θ is the angle between $\boldsymbol{B_0}$ and $\boldsymbol{B_1}$.

The optimal RF coil structure was acquired by comparing sSNR; optimal structure corresponds to maximum sSNR. Usually, the optimal structure was acquired by implementing UD for several rounds. In new UD round, experiment domain was reduced and optimal parameter in last round becomes the center in new experimental domain. Optimization ends when sSNR of RF coil no longer becomes larger.

3. Results

3.1. Magnet optimization

We designed and built a prototype of NMR probe in this work. The magnet of the probe was constrained in a cylindrical volume with height of 100 mm and diameter of 40 mm; the ROI of the probe is a ring at a radial distance of 25 mm from the cylinder axis; the depth along radial direction is 5 mm, and the height along axis is 10 mm. Considering that magnetic field strength and homogeneity, in ROI, were affected by each other, we optimized magnet structure with different constraint of standard deviation σ, the result was shown as Table 3. Where average B_0 is the average magnetic flux density of test points in ROI.

Fig. 5 shows that the average magnetic flux density, in ROI, increases with the increasing of the standard deviation σ. In other word, magnetic field strength is negatively related to magnetic field homogeneity in ROI. Fig. 6 shows the relationship between the optimal structure parameters and σ. With the increase of σ from 0.03 to 0.08, D_1 changed from 30.7381 mm to 35.9274 mm, increased by 6.88%; H_1 changed from 65.1774 mm to 43.8153 mm, reduced by 32.78%; D_2 remained unchanged; H_2 changed from 17.4113 mm to 28.0924 mm, increased by 61.35%.

Finally, we chose the optimal structure obtained with the standard deviation σ = 0.05. Fig. 7(a) shows magnitude and vector distribution of magnetic field of optimal magnet, acquired by FEM simulation in ANSYS Maxwell. Fig. 7(b) shows that measured by gaussmeter (BELL-8030, F. W. Bell, Inc.) with resolution of 1 mm, the measured gradient in ROI is 1.02 T/m. Fig. 7(c) shows the measuring platform. The analyzing district corresponds to the rotating plane in Fig. 3.

3.2. RF coil optimization

The design and optimization of RF coil is based on magnet structure, and the magnet was protected by a plastic shell

Table 3
Optimization result.

σ	0.03	0.04	0.05	0.06	0.07	0.08
Average B_0 (mT)	18.7977	22.9612	25.7175	27.7457	29.3452	30.6699
D_1 (mm)	30.7381	32.9546	34.1706	34.9506	35.5062	35.9274
H_1 (mm)	65.1774	57.4294	52.3865	48.7948	46.2072	43.8153
D_2 (mm)	40.0000	40.0000	40.0000	40.000	40.0000	40.0000
H_2 (mm)	17.4113	21.2853	23.8067	25.6026	26.9864	28.0924
Minimum B_0 (mT)	18.7348	22.8722	25.6068	27.6118	29.1883	30.4875
Maximum B_0 (mT)	18.8786	23.0717	25.8589	27.9133	29.5369	30.8875

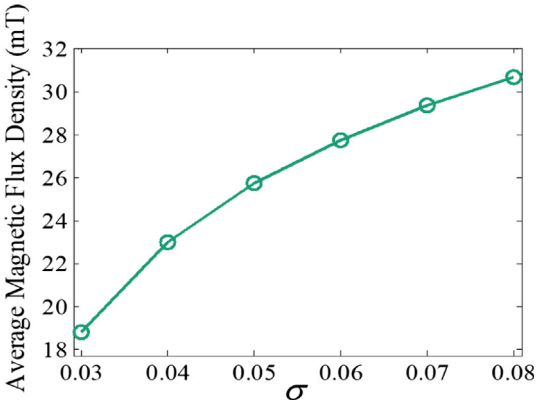

Fig. 5. The relation between average flux density in ROI with standard deviation of magnetic field in ROI.

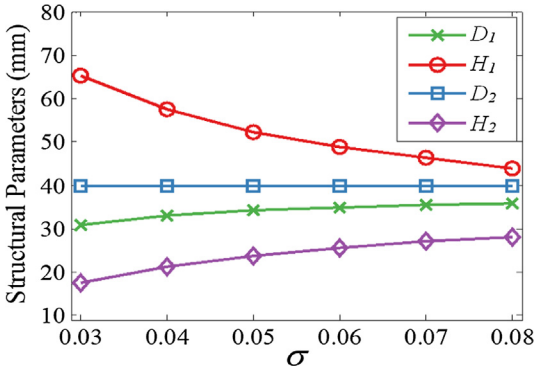

Fig. 6. The relation between structural parameter of magnet with standard deviation of magnetic field in ROI.

(diameter: 44 mm), made by 3D printer. The RF coil was wound around the plastic shell with a diameter of 44 mm. The optimization was carried out based on FEM simulation which was also implemented in ANSYS Maxwell for this work.

Simulation models of RF coil are shown as Fig. 8. Fig. 8(a) is the model of RF coil. Because FEM simulation of the full 3D model is computationally demanding and outside the resources of a typical desktop computer, we simplified the RF coil to several rings, shown as Fig. 8(b), then, the simulation model becomes a solid of revolution; FEM simulation of a 3D solid of revolution could be converted to a 2D simulation, which can be solved much more efficiently. The RF coil was simulated with the 2D model, shown as Fig. 8(c) on a desktop computer with result obtained in about 15 min.

Based on FEM simulation results, RF coil parameters, *X1*, *X2* and *X3* were optimized with 3-round UDs. The first round UD was implemented as the example in 2.1; the experiment domain, levels, and UD table were shown as Tables 1 and 2; after that, two more rounds of UDs were implemented. We arranged the sSNRs of every round of UD from small to large, shown as Fig. 9. Basically, sSNRs did not increase after 3-round UDs, and optimal structure parameters of RF coil were that correspond to the maximum sSNR in 3-round UDs. The optimal structure parameter is shown as Table 4. FEM simulation was conducted to study the magnetic field distribution of the optimal RF coil; Fig. 10 shows vector and magnitude distribution of RF magnetic field; Fig. 11 shows vector distribution of static and RF magnetic field of the probe.

Considering that saddle coil geometry is usually exploited on inside-out NMR probe, we compared the performance of a typical saddle RF coil whose structure is presented in [26] with our optimal opposed-solenoid RF coil. Fig. 12(a) shows the diagram of saddle coil (number of turns = 4; radius of the coil = 19.5, L = 28, h = 15.2, w = 0.6, d_1 = 1.2, d_2 = 2; unit: mm). Fig. 12(b), (c) show magnitude distribution of $\boldsymbol{B_1}$ on cross section of ROI. $\boldsymbol{B_1}$, generated by optimal RF coil, is the same at a certain depth, it is more homogeneous than that of saddle coil on the cross section, which could be found by comparing the scale of colour bar in Fig. 12(b), (c).

Moreover, we evaluate the performance of RF coil according to sSNR: the sSNR of saddle RF coil and the optimal RF coil was compared and the result was presented in Fig. 13. We chose three sampling circles, shown as Fig. 12(a), and calculated sSNR of RF coils at these 3 circles. According to the result, sSNR of NMR signal, measured by optimal coil, is the same at a certain depth, while that, measured by saddle coil, vary with circumferential angle θ, and at most parts of sampling circles, sSNR of optimal coil is larger than that of saddle coil. Therefore, the volume in ROI excited by optimal coil is larger that of saddle coil, and the SNR of NMR measurement of optimal coil can also be larger.

3.3. NMR probe

The prototype of NMR probe was built according to the optimal structure of magnet and RF coil, shown as Fig. 14(a). Fig. 14(b) shows the tuning and matching circuit, where C_m is the matching capacitor and C_t is the tuning capacitor, L_{coil} and R_{coil} is the equivalent inductance and resistance of RF coil.

4. Soil moisture measurement experiment

In order to verify the design and optimization of the probe, a soil moisture content experiment was conducted. The sample under study was natural river sands (particle diameter: 0.4–1.0 mm), shown as Fig. 15(a). The moisture content w, defined as equation (9), where m_1 is the mass of water, and m_2 is the mass of sands.

$$w = \frac{m_1}{m_{1+}m_2} \times 100\% \tag{9}$$

The samples with moisture content of 5%, 10%, 15% were measured in a beaker by the probe respectively. NMR signal was measured with hardware system shown in Fig. 15(b), including laptop, duplexer (1–2 MHz, Magritek Inc.), spectrometer (Kea2, Magritek Inc.) and RF power amplifier (BT00500 ALPHA-SA, Tomco Inc.).

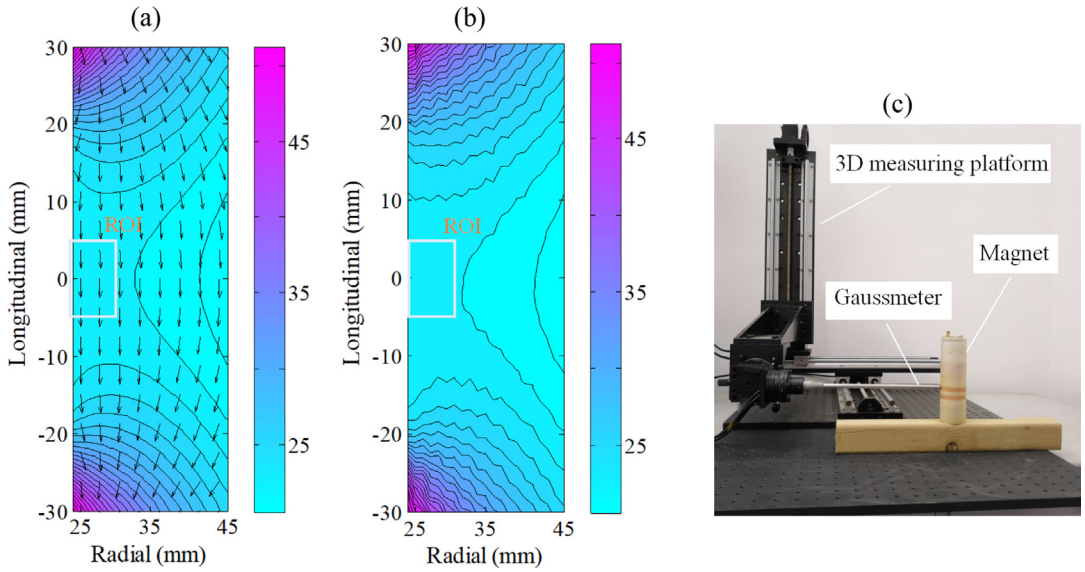

Fig. 7. Magnetic field distribution of magnet (B_0), the unit is mT. (a) Magnetic field distribution acquired by FEM simulation. (b) Magnetic field distribution measuring by gaussmeter. (c) 3D platform for magnetic field measuring.

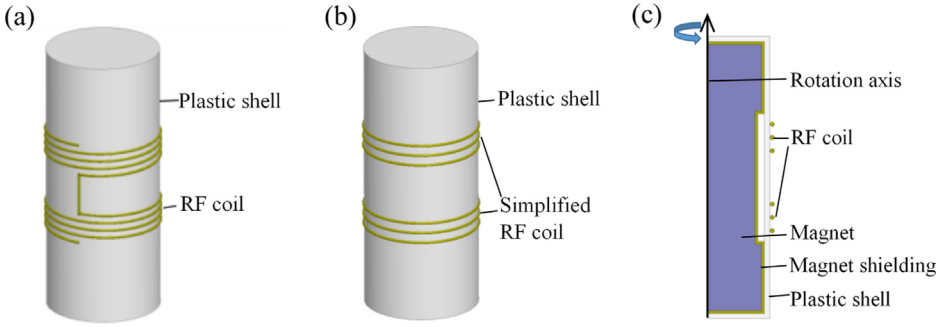

Fig. 8. FEM simulation model. (a) Actual model of RF coil. (b) Simplified RF coil model. (c) 2D model of RF coil for FEM simulation.

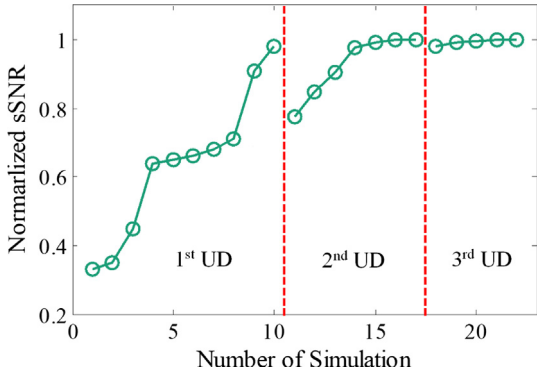

Fig. 9. sSNR comparison of simulations in 3-round UDs.

Table 4
Optimal RF coil structural parameter.

X1	*X2* (mm)	*X3* (mm)
3	14	0.6

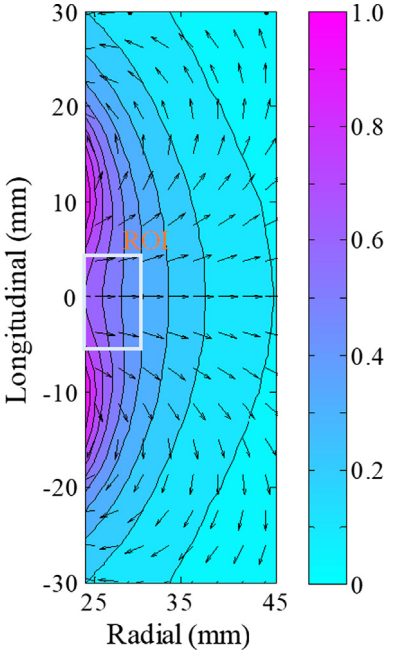

Fig. 10. RF magnetic field (B_1) distribution of optimal RF coil.

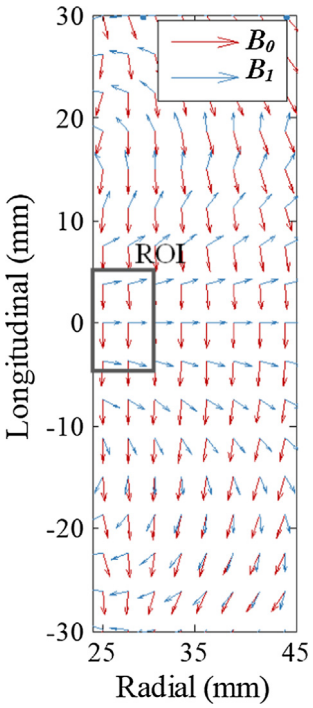

Fig. 11. Magnetic field distribution of the probe.

The NMR signal was obtained in 300 averages of a CPMG experiment; the 90◦ and 180◦ pulse widths are 24 μs, the NMR frequency is 1.08 MHz, the echo time is 200 μs, the time between two echos is 200 μs, the total echo number of one scan is 400, and the delay between 2 scans is 2.4 s. TR (time of repetition) is 3.2 s, and time for one experiment is 16 min. Fig. 16 shows CPMG decay curve measured from the sample with different moisture.

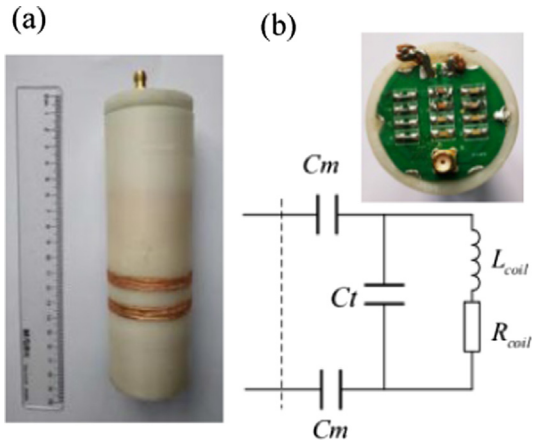

Fig. 14. NMR probe prototype. (a) The prototype. (b) Tuning and matching circuit.

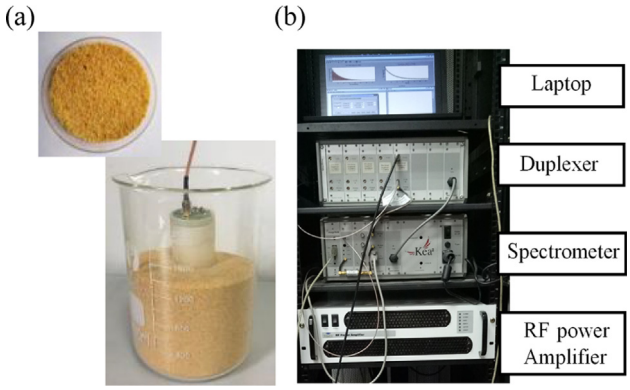

Fig. 15. NMR measuring experiment. (a) Sample for experiment (sands). (b) Hardware system for experiment.

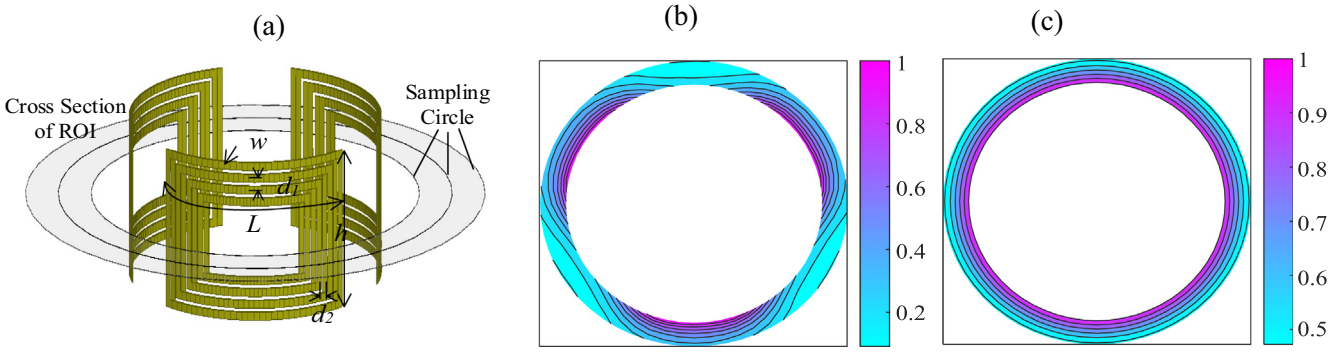

Fig. 12. (a) Diagram of saddle coil and 3 testing circle, L denotes the arc length, w denote coil width, d_1 and d_2 denote the gap between coils, h denotes the height of saddle coil, and the unit of radius is mm; (b) B_1 generated by saddle coil at cross section of ROI; (c) B_1 generated by optimized coil at cross section of ROI.

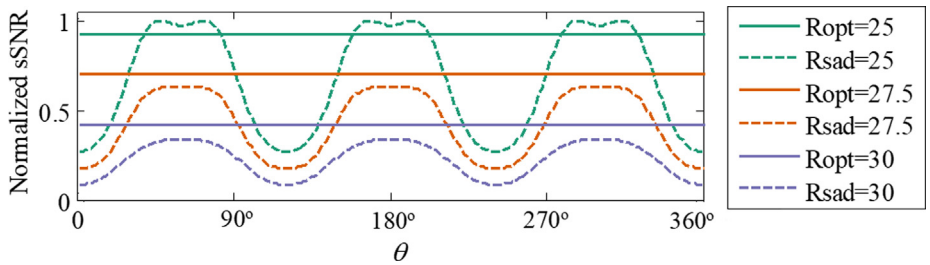

Fig. 13. sSNR comparison. Ropt denotes sSNR of optimized RF coil at a certain radius, Rsad denotes sSNR of saddl coil; the unit of radius is mm.

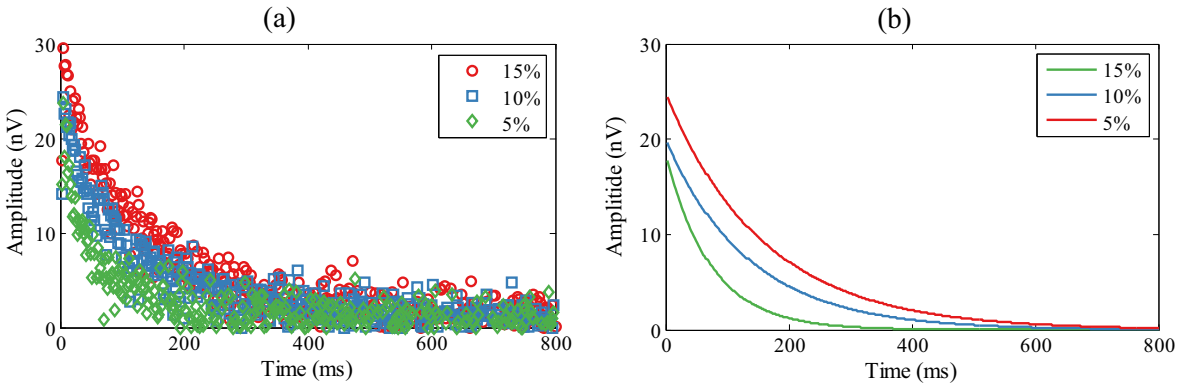

Fig. 16. CPMG decay curve. (a) Data measured by the prototype. (b) Fitting curve of data in (a), fitted by Contin. algorithm.

$$\text{Noise} = \sqrt{\left(\sum_{i=1}^{50} x_i^2\right)/50} \tag{10}$$

The SNR of NMR measurement was shown in Table 5, which is calculated by taking the ratio of the calculated signal and noise. The signal was calculated as the maximum of a moving average of 3 points. For the noise , last 50 echos x_i was chosen, and noise was calculated by Eq. (10). Basically, SNR was reduced with moisture content decrease.

The CPMG decay curves were further analyzed and the results were shown in Fig. 17. Fig. 17(a) shows the inverse Laplace transformation result of CPMG decay curves (Contin inversion routine).

Two kinds of peaks could be observed in Fig. 17(a), the peaks marked by Peak2 decrease and move toward left along as the moisture content of sand decreases, while the peaks marked by Peak1 change only slightly. The interpretation of NMR signal has been studied extensively: Andrada [34] classified water into 3 states, free water, weakly bound water and bound water; peak distribution reflects different states of water in sample, the water whose signal peak is located in the right in T_2 distribution spectrum is more freer than that whose signal peak is located in the left [35]. In our work, water in sands could be classified into free water which exist in the pore of sands and bound water which exist on the particle surface of sands. The signal of Peak1 is from bound water and the signal of Peak2 is from free water. With moisture content decrease, Peak1 shows no apparent change; while the amplitude of Peak2 decreased; the location of Peak2 move toward left which indicates water-state change, and this could be used to infer the reduction of pore size between sands.

Table 5
SNR of NMR measurement.

Moisture Content	5%	10%	15%
SNR	14.47	16.05	19.47

The water state was analyzed according peak distribution in T_2 distribution spectrum, the research published in [36,37] indicate peak area in T_2 distribution spectrum is proportional to moisture content in the sample. We analyzed peak area of T_2 distribution spectrum in Fig. 17(a) and the results were presented in Fig. 17(b). Basically, with moisture content decrease from 15% to 5%, the peak area of peak1 remain unchanged, and peak area of peak2 decreased, which indicates that only free water content was affected when moisture content decreased from 15% to 5%. We also analyzed the relation between total moisture content in sample and total area of T_2 distribution spectrum, according to

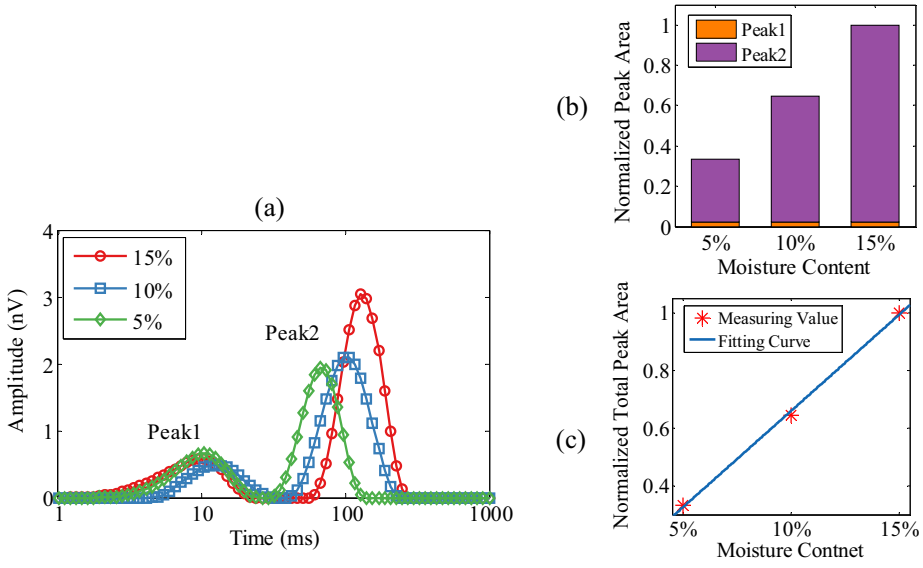

Fig. 17. Analysis of NMR signal. (a) T_2 distribution spectrum (Contin inversion routine). (b) Peak area of T_2 distribution spectrum, Peak1 relates to short T_2 peak and $Peak_2$ relates to long T_2 peak. (c) Relation between moisture content and total peak area of T_2 distribution spectrum.

the linear fitting result in Fig. 17(c), basically, the peak area is proportional to the moisture content.

5. Discussion

The application of the equivalent magnetization current method greatly increased the efficiency of optimization of magnet structure. However, this method was limited by the shape of magnet. Magnet designs with regular shapes, such as cylinders, cuboids, could be efficiently optimized with this method, while irregular-shape magnet may not, because the irregular shape makes it difficult to build an equivalent magnetization current model. As for the optimal magnet in this paper, we compared the magnetic fields of it acquired by FEM simulation and measuring; basically, these results were matched to each other, although the measuring magnetic field is not absolute symmetric. In this paper dumbbell-shape magnet was built by installing 3 cylindrical magnets in series. Imperfect coaxiality of magnets could results in the error of measuring magnetic field.

In RF coil optimization, only the magnetic field distribution and AC resistance were considered. However, wire of RF coil, inductance of RF coil and parameters of tuning and matching circuit would also influence the performance of NMR measuring. In this work, RF coil was made by litz wire which could effectively reduce eddy current effect and reduce AC resistance. Under the frequency of 1.08 MHz, the measured AC resistance of our RF coil is 126 mΩ. We also compared the AC resistance between RF coils which are made by litz wire and normal enamelled wire with both wire diameters being 1 mm. AC resistance of RF coil made by litz wire is reduced by 25% than that made by normal enamelled wire. Measured inductance of RF coil in this work is 0.64 μH, which determines the capacitor value of tuning and matching circuit with AC resistance; the tuning capacitor (C_t) is 32.5 pF, and the matching capacitor (C_m) is 4.17 pF. In general, C_t and C_m is sensitive to the value of inductance. Small inductance results in large C_t and C_m, and large inductance results in small C_t and C_m. Unfortunately, both circumstances would bring trouble in tuning and matching for RF coil. Small inductance or capacitors could be easily affected by the measuring environment and that would result in off-resonance of tuning and matching circuit. So, in RF coil optimization, proper limitation of inductance should be considered according to NMR measuring environment.

For RF coil optimization, UD was applied as a method to improve the efficiency. However, compared to analytic method, all the methods relating to FEM simulation are time-consuming for RF coil design. In the future, we will study fast computational method for the RF magnetic filed induced by RF coil, which will further improve the optimization speed.

Our soil moisture measuring experiment used an intentionally simple sample, as this choice of sample makes it easy to evaluate the performance of the NMR measurement. According to the results, only the signal corresponds to bound water was not distinguished with the change of moisture content. On the one hand, that indicates bound water states were changed very slightly, on the other hands, that also reveal the limitation of the NMR measuring. Objectively, NMR measuring was affected by NMR probe, hardware system, measuring parameter settings and measuring environment. In this paper, we could only evaluate the NMR probe qualitatively according to the experiment, measuring the moisture content of sands.

6. Conclusion

In this paper, we proposed a novel structure of inside-out NMR probe for soil moisture measuring and optimization methods for the structure of magnet and RF coil of the probe. The function of NMR probe with an optimized structure was demonstrated by soil moisture experiment. As this paper mainly focused on a novel structure of inside-out NMR probe and its optimization, further experiments with this NMR sensor are beyond the scope of this paper; and that would be studied in our future work. Moreover, a larger probe with same structure in this paper would be built and the application of the probe would be extended to well logging.

Acknowledgements

This research was funded by the National Natural Science Foundation of China (No. 51677008 and 51707028), Fundamental Research Funds for the Central Universities (No. 2018CDJDDQ0017), and Science and Technology Funds of Chongqing Municipal Education Commission (KJ1600333). Sincere thanks to Prof. Matthew Scott Rosen from Harvard Medical School for his help and precious suggestion on paper revising.

References

[1] B.M. Das, Principles of Geotechnical Engineering, fifth ed., Thomson, Bangalore, India, 2004.
[2] R.F. Craig, Craig's Soil Mechanics, E and FN Spon, London, 2005.
[3] L.D. Baver, Soil Physics, John Wiley and Sons, New York, 1956.
[4] H.G. Jones, Plant water relations and implications for irrigation scheduling, Acta Horticult. 278 (1990) 67–76.
[5] A.M. Michael, T.P. Ojha, Principles of Agricultural Engineering:Agricultural Surveying, Irrigation, Agricultural Drainage, Soil And Moisture Conservation, Jain Brothers, New Delhi, 1996.
[6] T.A. Howell, Enhancing water use efficient in irrigated agriculture, Agron J. 93 (2) (2001) 281–289.
[7] F. Pan, Estimating daily surface soil moisture using a daily diagnostic soil moisture equation, J. Irrigation Drain. Eng, ASCE. 138 (1) (2011) 625–631.
[8] D.A. Robinson, S.B. Jones, J.M. Wraith, J. Or, F.P. Friedman, A Review of advances in dielectric and electrical conductivity measurement in soils using time domain reflectometry, Vadose Zone J. 2 (2003) 444475.
[9] R. Saksena, S. Chandra, B.P. Singh, A gamma transmission method for the determination of moisture content in soils, J. Hydrol. 23 (1974) 341–362.
[10] W. Daily, A. Ramirez, A. Binley, D. LaBrecque, Electrical resistance tomography theory and practice, in: D.K. Butler (Ed.), Near-Surface Geophysics, Investigations in Geophysics, vol. 13, Society of Exploration Geophysicists, Tulsa, 2005, pp. 525–550.
[11] J. Bear, Dynamics of Fluids in Porous Media, third ed., Dover, New York, 1988.
[12] R.K. Cooper, J.A. Jackson, Remote (inside-out) NMR: I. Remote production of a region of homogeneous magnetic field, J Magn Reson 41 (3) (1980) 400–405.
[13] L.J. Burnett, J.A. Jackson, Remote (inside-out) NMR: II. Sensitivity of NMR detection for external samples, J. Magn. Reson. 41 (3) (1980) 406–410.
[14] J.A. Jackson, L.J. Burnett, F. Harmon, Remote (inside-out) NMR: III. Detection of nuclear magnetic resonance in a remotely produced region of homogeneous magnetic field, J. Magn. Reson. 41 (3) (1980) 411–421.
[15] R.L. Kleinberg, A. Sezginer, D.D. Griffin, et al., Novel NMR apparatus for investigating an external sample, J. Magn. Reson. 97 (3) (1992) 466–485.
[16] R.N. Chander, E.D. Drack, M.N. Miller, et al., Improved log quality with a dual-frequency pulsed NMR tool, The 69th Annual Technical Conference and Exhibition of the Society of Petroleum Engineers, New Orleans, 1994.
[17] C.C. Mirth, D. Davies, D. Mckeon, et al., An improved NMR tool design for faster logging, SPWLA 40th Annual Logging Symposium, Society of Petrophysicists and Well-Log Analysts, 1999.
[18] N.J. Heaton, R. Freedman, C. Karmonik, et al., Applications of a new-generation NMR wireline logging tool, SPE Annual Technical Conference and Exhibition, Society of Petroleum Engineers, 2002.
[19] M. Borghi, F. Porrera, A. Lyne, et al., Magnetic resonance while drilling streamlines reservoir evaluation, SPWLA 46th Annual Logging Symposium. HHH; June 26–29, 2005.
[20] O. Sucre, A. Pohlmeier, A. Minière, B. Blümich, Low-field NMR logging sensor for measuring hydraulic parameters of model soils, J. Hydrol. 406 (2011) 30–38.
[21] R.J.S. Brown, B.W. Gamson, Nuclear magnetism logging, Pet Tech. 219 (1960) 199–207.
[22] R.J.S. Brown, B.W. Gamson, Nuclear magnetism logging, Pet Tech. 219 (1960) 349–353.
[23] G.A. Matzkanin, R.F. Paetzold, Measuring Soil Water Content Using Pulsed Nuclear Magnetic Resonance, ASAE Winter Mtg., Paper No.82-2619, Chicago, Illinois, 1982.
[24] M. Meju, P. Denton, Fenning, Surface NMR sounding and inversion to detect groundwater in key aquifers in England: comparisons with VESTEM methods, J. Appl. Geophys. 50 (2002) 95111.
[25] J. Perlo, E. Danieli, et al., Optimized slim-line logging NMR tool to measure soil moisture in situ, J. Magn. Reson. 233 (2013) 74–79.

[26] J. Wu, P. Guo, S. Shen, M. Mini, et al., Inside-out nuclear magnetic resonance sensor design for soil moisture measurements, Sensors 19 (7) (2019) 1682, https://doi.org/10.3390/s19071682.
[27] A.E. Marble, I.V. Mastikhin, B.G. Colpitts, B.J. Balcom, A compact permanent magnet array with a remote homogeneous field, J. Magn. Reson. 186 (2007) 100–104.
[28] S.L. Luo, L.Z. Xiao, et al., Design of an innovative downhole NMR scanning probe, IEEE Trans. Geosci. Remote Sens. 57 (5) (2018) 2939–2946.
[29] S. Tumanski, Induction coil sensors—A review, Meas. Sci. Technol. 18 (3) (2007).
[30] H.M. Kim, G.S. Park, A new sensitive excitation technique in nondestructive inspection for underground pipelines by using differential coils, IEEE Trans. Magn. 53 (11) (2017) 1–4.
[31] D.I. Hoult, R.E. Richards, The signal-to-noise ratio of the nuclear magnetic resonance experiment, J. Magn. Reson. 24 (1) (1976) 71–85.
[32] J.D. Jackson, Classical Electrodynamics, 3rd ed., John Wiley & Sons, Inc., Hoboken, NJ, USA, 1999, pp. 184–194.
[33] K.T. Fang, D.K.J. Lin, Ch. 4. Uniform experimental designs and their applications in industry, Handbook Stat. 22 (2003) 131–170.
[34] Heber E. Andrada, María B. Franzoni, Alejo C. Carreras, Fabián Vaca Chávez, Dynamics and spatial distribution of water in Nafion 117 membrane investigated by NMR spin-spin relaxation, Int. J. Hydrogen Energy 43 (18) (2018) 8936–8943.
[35] K. Bauer, J. Kulenkampff, J. Henninges, E. Spangenberg, Lithological controls on gas hydrate saturation: insights from signal classification of NMR downhole data, EGU General Assem. Conf. Abs. 18 (2016) 13152.
[36] A.T. Krzyżak, I. Habina, Low field 1H NMR characterization of mesoporous silica MCM-41 and SBA-15 filled with different amount of water, Microporous Mesoporous Mater. 231 (2016) 230–239.
[37] W. Lv, M. Zhang, B. Bhandari, et al., Smart NMR method of measurement of moisture content of vegetables during microwave vacuum, Drying Food Bioprocess Technol. 10 (2017) 2251, https://doi.org/10.1007/s11947-017-1991-3.